Quantum Dot Photoluminescence Activation and Decay: Dark, Bright, and Reversible Populations in ZnS-Capped CdSe Nanocrystals

Mark A. Osborne[†,§,*] and Steven F. Lee[‡,§]

[†]School of Life Sciences, Department of Chemistry, University of Sussex, Falmer, Brighton BN1 9QJ, United Kingdom and [‡]Chemistry Department, University of Cambridge, Lensfield Road, Cambridge CB2 1EW, United Kingdom. [§]Authors contributed equally to this work.

ABSTRACT Semiconductor nanocrystals or quantum dots (QDs) exhibit a number of unique optical properties including fluorescence intermittency (FI), photoluminescence (PL) enhancement, and darkening. Here we report PL activation (PLA) and darkening over populations of single colloidal ZnS-capped CdSe QDs under continuous illumination, which is described well by a simple consecutive elementary reaction (CER) scheme in the 1 to 10 kW cm^{-2} excitation intensity regime. The scheme allows determination of rate constants for both fluorescence activation and decay processes as well as the measurement of initial bright, fluorescent and dark, nonfluorescent QD fractions. The latter parameters can function as a "quality control" on the total population of detectable QDs in an imaging experiment or a synthesis. We further show reversible PLA at low intensities < 0.5 kW cm^{-2} and a photoinduced conditioning of the QD that results in increased rates of PLA following repeated cycles of illumination and an induction period that precedes photoactivation upon initial exposure to light. By interrogating individual QD fluorescence trajectories, the population fractions found exclusive to each of three illumination cycles, common to any two cycles and fluorescent in all three cycles, show that only a small number of QDs (~5%) remain fluorescent through multiple cycles of photoactivation and recovery.

KEYWORDS: quantum dots · photoluminescence activation · photodarkening · power dependency · wavelength dependency · reversible activation · elementary reactions

Colloidal semiconductor nanocrystals, or quantum dots (QDs), have become essential light-harvesting and light-emitting components across a range of applications from biosensing, cell imaging, and diagnostics[1−3] to optical storage,[4,5] solar cells,[6] and display technologies.[7] As fluorescent probes, they possess high extinction coefficients and quantum yields, narrow band emission, and generally superior photostability compared to conventional organic fluorophores. However, for all of the benefits QDs offer, they exhibit a number of photophysical properties that are not well understood and can be detrimental to their utility. For example, the on−off blinking associated with fluorescence intermittency (FI)[8,9] reduces the steady-state, ensemble quantum yield (QY)[10] which may manifest as flickering in the emission intensity at low QD concentrations.[11] Furthermore, FI will result in the loss of information in FRET[12] and particle tracking[13] experiments during dark, nonfluorescent periods. On the other hand, photoactivation of the ensemble[14,15] coupled with photoluminescence enhancement (PLE) at the single QD level[16] will add uncertainty to the quantitative measurement of QD numbers, in cellular imaging[17] or biosensing,[18] for example.

In general, samples of as-prepared nanocrystals contain a not insignificant fraction of dark, nonfluorescent QDs under ambient conditions. In particular, ZnS-capped CdSe nanocrystal conjugates have been shown to contain as much as 75% fluorescently inactive QDs, depending on the lot.[19,20] This dark fraction has been attributed to a slow ionization and charge carrier trapping that prohibits normal radiative electron−hole recombination in the QD core, even at low light levels.[21] Under continuous illumination, the nonfluorescent fraction is transformed to a fluorescently active state, resulting in the overall PLE of the ensemble. A number of PLE studies on CdSe nanocrystals have attributed enhancement to the passivation of exciton traps by adsorbates[22,23] or surface state transformations,[24] Coulomb blockade effects,[25] and internal electric field effects.[26,27] Recent observation of a superlinear correlation between PL intensity and the number of fluorescent QDs has allowed the distinction between PL enhancement (decay) due to activation (bleaching) of the dark (bright) population and that due to genuine change in the QY of individual QDs.[16] Subsequent analysis of single QD intensity trajectories identified a number of distinct

* Address correspondence to m.osborne@sussex.ac.uk.

Received for review August 6, 2011 and accepted September 18, 2011.

Published online September 18, 2011
10.1021/nn202994w

phenomena including activation, brightening, FI, spectral bluing, and photobleaching over the photochemical lifetime of the QD.[28]

We report the observation of PL activation and decay over the photochemical lifetime of a population of water-soluble, ZnS-capped CdSe nanocrystals, under continuous illumination. By measuring changes in the absolute population of fluorescent QDs, independent of individual PL intensities, we differentiate between PL activation (PLA) from PL enhancement (PLE) resulting from changes in the QY of individual QDs. The temporal evolution of the fluorescent fraction is described quantitatively well by a simple, two-step, consecutive elementary reaction (CER) scheme from which the initial dark and bright QD populations can be extrapolated. A systematic study of the power dependence of these two quantities finds their sum, the total number of detectable QDs, to be independent of power. The fluorescent fraction, as a ratio of the total population, may then provide a useful "quality control" measure for the optimization of a QD synthesis or imaging conditions for the maximum observable QD population. Additionally, the CER scheme allows determination of the rates of photoactivation and photodarkening (bleaching) from which excitation intensity and wavelength dependencies have been derived over the ranges 1−10 kW cm^{-1} and 457−514 nm, respectively. While the radiation dose in this power regime results in apparent irreversible darkening (photobleaching), below ~0.5 kW cm^{-1}, we observe reversible PLA following a limited illumination time and period of recovery in the dark. By measuring numbers of individual fluorescent QDs, we compare the evolution of the fluorescent population over multiple cycles of illumination and recovery to the absolute photoactivation times of single QDs, extracted from individual intensity trajectories. Furthermore, by colocalizing molecules and tracking trajectories across multiple cycles, we identify populations unique to each cycle, common to pairs of cycles, and those QDs that remain fluorescently active through three full illumination/recovery cycles. Quantitative analysis of the PL activation and decay kinetics within the CER scheme reveals increased rates of activation with repeated excitation cycles. Moreover, at the lower excitation intensity, growth in the fluorescent QD population in the initial cycle was found not to fit well within the CER scheme but was more characteristic of an autocatalytic-like process. We attribute an induction period observed in the initial cycle of PLA to the conditioning of the QD *via* mutually enhancing processes normally associated with FI, namely, ionization and passivation.

RESULTS AND DISCUSSION

Power Dependence of PL Kinetics. To investigate the power dependence of PL activation and decay,

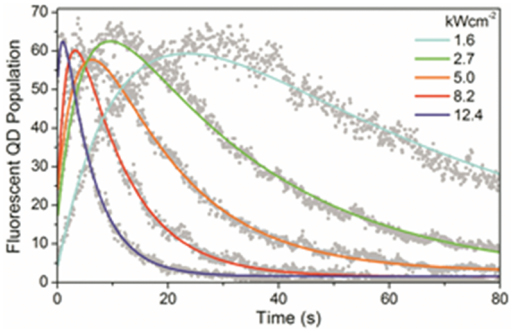

Figure 1. Evolution of the fluorescent QD population with time (gray points) at different excitation intensities and fixed laser wavelength λ = 488 nm. Superimposed are nonlinear least-squares fits (colored lines) of the consecutive elementary reaction (CER) eq 1. The kinetics of the QD population were analyzed for over 300 s, but profiles have been truncated for clarity.

fluorescence from large populations of single QDs was monitored under TIRF with continuous illumination, at a fixed wavelength of 488 nm, over the excitation intensity range of 1.2−12 kW cm^{-2}. In this regime, enhancement in the number of fluorescent QDs was observed to compete with photobleaching of the population at all power densities, resulting in the temporal QD population traces displayed in Figure 1. The power dependence in both the rates of population increase and decrease is immediately evident from the narrowing of the kinetic profiles at higher excitation intensities. Control samples in which all QDs have been photobleached showed no recovery in fluorescence over a period of up to 300 s of intermittent excitation and imaging. This provides a working definition of the photobleached population in this case but does not negate the possibility that FI leads to QDs residing in dark, nonfluorescent states for periods extending well beyond the experimental window.

The kinetics of activation and decay in the fluorescent QD population can be described succinctly by a consecutive elementary reaction (CER) scheme of the form A → B → C. In this case, a dark QD state A evolves *via* photoactivation with a rate constant k_a into the fluorescent intermediate B, before decaying with a rate constant k_d to a nonfluorescent product C. In general, for a chemical reaction scheme of this type, there is no initial population of the intermediate, $B_0 = 0$ at $t = 0$, resulting in a time evolution of the population $B(t)$ dependent only on the initial dark population A_0. In this instance B_0 is nonzero, and the solution to the first-order rates in populations A, B, and C gives[16]

$$B(t) = A_0 \frac{k_a}{k_d - k_a} (e^{-k_a t} - e^{-k_d t}) + B_0 e^{-k_d t} \quad (1)$$

The function has been fitted to the time evolution of the fluorescent QD population, for each excitation intensity, using a nonlinear least-squares Levenberg−Marquardt minimization within experimental error (standard deviation of a 3 × 3 sampling array).

TABLE 1. Power Dependence of the Initial Dark, Nonfluorescent QD Population, A_0, and Bright, Fluorescent Population, B_0, with Rates of Photoactivation, k_a, and Population Decay, k_d

				k_a (s^{-1})	k_d, s^{-1}	
I, kW cm^{-2}	χ^2	A_0[a]	B_0[a]	($\sigma \times 10^{-1}$)[a]	($\sigma \times 10^{-3}$)[a]	$A_0 + B_0$
12.4	0.09	31 (15)	49 (16)	1.3 (8)	0.182 (9)	82 (22)
8.2	0.15	67 (5)	19 (5)	0.55 (0.9)	0.107 (5)	87 (7)
6.3	0.40	59 (5)	22 (4)	0.42 (0.7)	0.055 (3)	80 (6)
5.0	0.13	68 (4)	20 (4)	0.25 (0.3)	0.058 (2)	88 (5)
2.7	0.11	72 (3)	13 (3)	0.21 (0.2)	0.0328 (0.5)	85 (4)
1.6	6.00	87 (1)	1.8 (0.5)	0.081 (0.02)	0.0182 (0.3)	88 (1)

[a] Parameters (standard deviation in brackets) determined from nonlinear least-squares fit of the consecutive elementary reaction (CER) eq 1 to experimental data in Figure 1 following reduced χ^2 minimization.

The resulting curves are superimposed on the experimental data in Figure 1 with the parameters A_0, B_0, k_a, and k_d presented in Table 1. Incorporation of backward rates to allow equilibria between initial dark, bright, and photodarkened (photobleached) states was found not to improve fits (data not shown) but significantly complicated the integrated rate expressions and fitting. It is important to reiterate here that, by performing experiments on dispersions of single, isolated QDs, the absolute populations of the fluorescently active B state have been measured by directly counting QDs, and thus kinetics of PL activation and decay are independent of the changes in the QY of individual QDs.

Evidently, the initial bright, fluorescent population B_0 and dark, nonfluorescent QD population A_0 are strongly anticorrelated, exhibiting positive and negative dependencies on the excitation intensity, respectively, as presented in Figure 2a. More importantly, the sum of A_0 and B_0 is found to remain largely constant over the entire range of illumination intensities. This indicates that the fraction of QDs with the potential to undergo photoactivation is fixed, that no additional dark QDs are activated at increasing excitation powers, and that the observed fluorescent fraction is solely dependent on the radiation dose (intensity $\times$ exposure time), all other conditions being equal. Alternatively, for a fixed excitation dose, the initial bright fraction $B_0/(A_0 + B_0)$ serves as a measure of the "quality" of a QD sample under variable experimental conditions. We note that this method of measurement complements other techniques for identifying dark and bright fractions that effect QD brightness.[10,18,20,29] Such a measure may prove useful in a number of applications, for example, in comparing the quality of different QD syntheses, either batch-to-batch under the same conditions or *via* different routes. Moreover, the detrimental effect of PL instabilities in quantitative live-cell imaging has been recognized.[30] Here, modeling with the CER would allow a quantitative estimate of the maximum number (PL intensity) of detectable QDs, as well as the total number under specific illumination

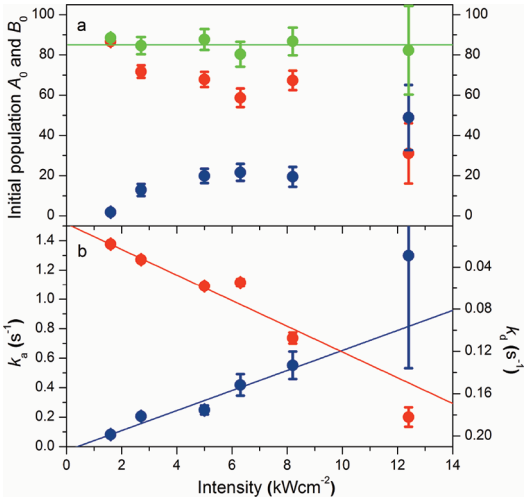

Figure 2. (a) Excitation intensity dependence of the initial dark population, A_0 (red), and bright population, B_0 (blue), and their sum $A_0 + B_0$ (green) as determined from the nonlinear least-squares fit of the consecutive elementary reaction (CER) eq 1 to the experimental data of Figure 1. (b) Rates of photoactivation k_a (blue + left axis) and decay k_d (red + right axis) both showing a linear dependency with excitation rate, at illumination intensities below saturation at ~10 kW cm^{-2}. Error bars represent the standard error determined from the minimized reduced χ^2 (Table 1), and covariance and lines are shown for guidance only.

conditions. In contrast, these instabilities have been exploited in the design of novel bio- and chemosensors.[31,32] Accurate measurement of analyte concentrations and binding constants in this case will likely depend on knowledge of the fluorescently active and inactive QD fractions. The fact that a dark fraction of QDs exists clearly has both advantages and disadvantages depending on the application.[28] Direct measurement of the quality of a QD sample could thus be used to optimize bright and dark fractions, either by synthesis or postfabrication modification, for quantitative imaging (all bright QDs), or improved sensitivity in biosensing by PL activation (mostly dark QDs). Application of this measurement is not limited to the life sciences but extends to photovoltaics in which QDs are increasingly used as sensitizers in solar cells. The effects of a significant dark fraction and PLA in this case may act to introduce a lag-time before maximum conversion efficiency is reached and likely constitutes the origin for the increased efficiency observed in QD solar cells following exposure to ambient light and atmospheric aging.[33]

Analysis of the rates of PL activation and decay shows a near linear dependence on the incident laser power, as seen in Figure 2b. The emergence of a nonlinear scaling may be evident at intensities in excess of 10 kW cm^{-2}, a power density at the lower limit of the single exciton saturation intensity for nanocrystals of this size.[34] Nonlinear behavior might be expected as multiexciton processes scale with excitation rates. Recent experiments on "giant" CdS-capped CdSe have

shown a contribution to the spectrally integrated PL from biexciton emission with a quadratic dependence on excitation power, although the total PL intensity was found to scale linearly with intensity in the range of 0.01−1 kW cm^{-2}.[35] If the biexciton emission does not saturate too rapidly at higher excitation rates, then the integrated PL would presumably become nonlinear with power as biexciton emission becomes dominant. More importantly, in consideration of the dark and bright state populations, recent evidence indicates that biexciton emission can contribute to a low intensity "gray state" following ionization of the QD,[36] a state normally considered nonfluorescent due to rapid Auger quenching of the monoexciton in the presence of core charge. If these "biexciton" gray states render otherwise dark QDs detectable, then this would likely contribute to enhanced B_0 and reduced A_0 values and effectively increase photoactivation rates. In addition, recent investigations of FI have revealed a quadratic power dependence of the role-off rate in the on-time probability distribution, a feature frequently observed in the power-law statistics of single QD blinking over extended time scales.[37,38] In this case, the nonlinear dependency was shown to be closely aligned with the characteristic rate of formation of multiexciton states. Given the evidence for a correlation between FI and PLE,[16,39] the participation of multiexcitons in the enhancement of the detectable QD population at higher excitation intensities may not be entirely unexpected here.

Wavelength Dependence of PL Linetics. The effects of excitation energy on PLA and degradation were investigated using the separate lines of an Ar ion laser at 457, 477, 488, 496, and 514 nm at a fixed intensity of 0.5 kW cm^{-2}. Evolution of the fluorescent QD population with time shows enhancement preceding decay in QD numbers at all wavelengths. Normalized traces for 514, 496, and 457 nm are shown in Figure 3, along with best fits of the modified CER equation. Qualitatively, it is evident that rates of PL activation and decay scale with excitation energy, reflecting the increased absorption coefficient at shorter wavelengths. Indeed rates of activation, k_a, and decay, k_d, extracted from the CER fit (Table 2) show good correlation with the bulk QD absorption band over the sampled range of wavelengths, as seen in the inset of Figure 3. Decay rates in this instance appear less sensitive to excitation energy above 496 nm than PL activation rates, which may suggest different mechanisms for QD photoactivation and photodegradation or at least different contributions from pathways that give rise to both of these processes.

For example, the photoactivation of QDs that leads to net PLE in ensemble studies has been attributed to the passivation of defects at the QD surface or capping interface by adsorbates, whether these be gases on thin QD films[14,39] or solutes in colloidal suspensions.[15,40] These defects act as potential trapping sites for the exciton associated charge carriers, biasing exciton

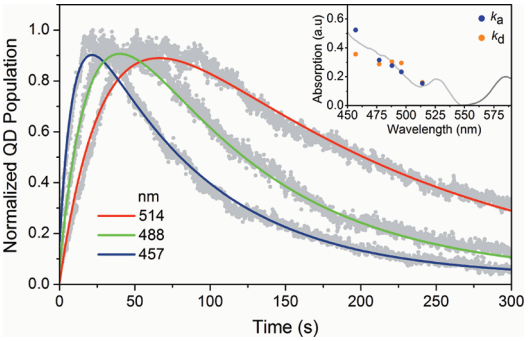

Figure 3. Evolution of the fluorescent QD population (gray points) with time at different excitation wavelengths and fixed laser intensity, 0.5 kW cm^{-2}. Superimposed are nonlinear least-squares fits of the consecutive elementary reaction (CER) eq 1 (colored lines). Kinetic profiles at 477 and 496 nm have been omitted for clarity. Inset: correlation between fluorescence activation and decay rates k_a and k_d and the UV−vis absorption profile with rates arbitrarily normalized to the relative absorption.

TABLE 2. Wavelength Dependence of the Initial Dark, Nonfluorescent QD Population, A_0, and Bright, Fluorescent Population, B_0, with Rates of Photoactivation, k_a, and Population Decay, k_d

λ, nm	χ^2	A_0[a]	B_0[a]	k_a, s^{-1} ($\sigma \times 10^{-3}$)[a]	k_d, s^{-1} ($\sigma \times 10^{-4}$)[a]
457	0.07	112 (3)	8.5 (3)	0.115 (6)	0.013 (2)
477	0.13	140 (3)	7.2 (2)	0.059 (3)	0.010 (3)
488	0.11	125 (2)	1.2 (1)	0.057 (2)	0.011 (3)
496	0.05	65.3 (2)	1.6 (1)	0.048 (3)	0.010 (6)
514	0.11	101 (2)	0.2 (0.4)	0.032 (2)	0.006 (6)

[a] Parameters (standard deviation in brackets) determined from nonlinear least-squares fit of the consecutive elementary reaction (CER) eq 1 to experimental data in Figure 3 following reduced χ^2 minimization.

relaxation toward nonradiative recombination events. In this case, the light-driven separation of charge carriers leads to an excited state dipole[41] that most likely induces charge solvation by the adsorbate, a model supported by the observation of a substantive reversible component in ensemble PLE[4,5,14] (see below). The energy dependence of the activation rate then simply reflects the increased absorption driving the equilibrium toward passivation. Conversely, PL decay is generally associated with photooxidation at the QD core surface,[29,42,43] which likely introduces further defects either through the loss of Cd and Se atoms in products such as CdO or SeO_x or *via* lattice mismatches between CdSe and compound oxides of the form $CdSeO_x$.[44] Ultimately, these defects dominate over any passivation by absorbates, leading to increased charge carrier trapping and hence increased probability of nonradiative recombination. In general, there will be an activation barrier between the physisorbed, passivating adsorbate and the chemisorbed oxide,[39] unless the adsorbate interaction lies within the chemisorption potential. An excitation energy threshold to photooxidation might then be expected, which may

account for the step-like change and insensitivity seen in the wavelength-dependent PL decay rates of Figure 3 (inset) above 514 nm. A drop in the oxidation rate at wavelengths approaching band-edge excitation is not wholly unexpected since excitation below the band-edge has been found not to induce photooxidation but does maintain some degree of photoactivation.[42]

Reversibility of PL Activation. The extent to which PLA and photodarkening of the QDs is reversible was investigated by performing a series of activation and relaxation cycles in which a QD sample was first monitored under continuous laser excitation at 514 nm and 0.25 kW cm^{-2} for a fixed period of 20 s, then left dark for an extended period of 160 s. The cycle was repeated to observe any recovery of the dark fraction and reactivation of the QDs. The initial radiation dose resulted in the number of fluorescent QDs peaking at ~80 QDs in a single frame, followed by approximately 90% recovery of the dark population by the end of the first cycle, as seen in Figure 4a. The second and third cycles of activation, under identical conditions, promote more rapid activation of the dark fraction, but only 75% and 44% of the peak fluorescent QD population of the first cycle is seen to be reactivated, respectively. Loss of the fluorescent fraction arises from either a QD population that remains ionized and darkened after the recovery time and/or an irreversibly photobleached population. Further examination of the activation curves shows the fluorescent population peaks within about 10 s after the second and third cycles, about half the time of the first cycle.

The observation suggests a preconditioning of the QDs in the first cycle that advances reactivation to shorter times in subsequent illumination cycles. Indeed, by interrogating individual QD fluorescence trajectories and measuring the distribution of lag-times before the onset of fluorescence, as presented in Figure 4b, it can be seen that the largest single fraction of molecules reactivates immediately (at least within 100 ms time resolution of our experiment) in both second and third cycles, while in the first cycle, QDs require an extended period of illumination before a significant population is photoactivated. The fluorescence trajectories of a single QD closely representing this behavior is presented in Figure 4c, while a trajectory reflecting the ensemble peak activation times is shown in Figure 4d. QDs that exhibit fluorescence throughout the three cycles are rare and constitute typically only 5% of the total number counted over the entire experiment. The lag-time to activation in the first cycle means that many QDs do not activate until the second (36%) or even third cycle (9%) and darkening or photobleaching removes many QDs (79%) by the end of the second cycle. The advantage of interrogating single QDs here is that the fluorescent population unique to each cycle, common to any two cycles and that present in all three cycles, can be determined by

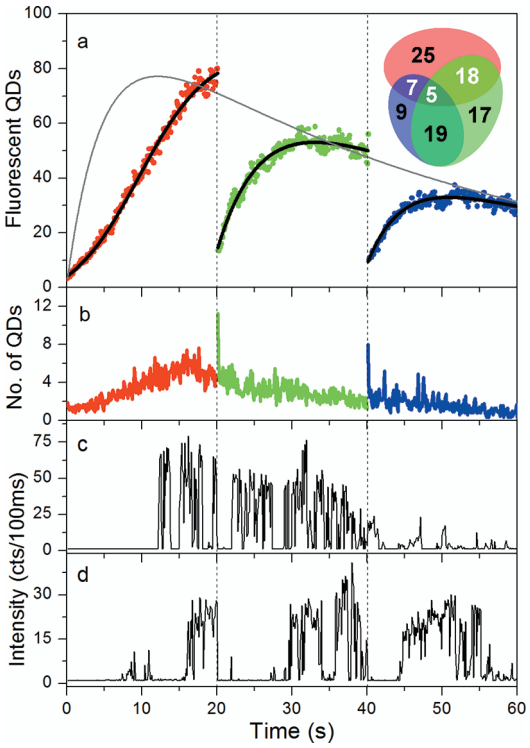

Figure 4. (a) Temporal evolution of the fluorescent QD population showing three cycles of PLA under continuous illumination and recovery of a nonfluorescent population following a period in the dark. Duration of each illumination cycle is 20 s at 514 nm and 0.25 kW cm^{-2} (ending at the dotted line) and that of the dark phase is 160 s (not shown). Inset: Venn diagram showing percentage populations of fluorescent QDs that appear uniquely in each cycle, are common between two cycles, and appear in all three cycles (averaged from a 2 × 2 experimental array). (b) Distribution of lag-times before photoactivation of individual QDs in each cycle. (c) Single QD fluorescence trajectory representative of the most probable photoactivation time from the peak of the PLA curves of (a). (d) QD trajectory closely aligned with the distribution of photoactivation lag-times in (b), showing near-instant reactivation of the QD following the initial photoinduced conditioning of the QD. Decay of the QY in this trajectory is also evidence of oxidation.

colocalizing molecules in images across all three cycles. We represent these average populations (as a percentage of the total number) by a Venn diagram, as shown in the inset of Figure 4a. The analysis shows the bright population in the second cycle (17 + 19 = 36%), following dark state recovery after the first cycle, arises primarily *via* photoactivation of a substantial fraction (36/45 = 80%) of the dark population (100−25−18−7−5 = 45%) that remains at the end of the initial illumination cycle. Only a small fraction of QDs (23%), fluorescent in the first cycle, are reactivated in the second cycle. Reactivation of QDs appearing in the first and second cycle (7 + 5 + 19 = 31%) forms the dominant fraction (31/40 = 78%) of the total population of QDs appearing in the third cycle (40%). It is worth noting that information on fluorescently active and reactivated populations under repeated cycles of illumination and dark phase recovery could prove useful

in the optimization of QD devices,[4−7] in particular for the measurement of aging in these devices.

Further analysis of the ensemble photoactivation reveals that fitting the activation curves in Figure 4a (black lines) with the standard CER scheme represented by eq 1 is only possible in the second and third phase of activation. Importantly, the effect of photoconditioning is highlighted by the fact that the first cycle exhibits a significant lag in the activation of the fluorescent QD population that cannot be fitted by the CER equation. Moreover, CER fits to the second and third cycles show initial rates of photoactivation increasing from k_a = 0.16 (0.01) s^{-1} to 0.22 (0.02) s^{-1} as QD conditioning continues through the second cycle of illumination. In the first cycle, the presence of an induction period and the resulting sigmoidal growth in the fluorescent QD fraction appears more characteristic of an autocatalytic process in which the conversion of reactant A to product B is catalyzed by product B itself. If we assign reactant A to the dark state and B to the fluorescent state, then the sigmoidal growth in the fluorescent fraction is described well by the solution to the second-order rate equation $dB/dt = k_cAB$ for the autocatalytic reaction A + B → 2B. In this case, fitting $B(t)$ to the QD photoactivation curve of the first cycle gives a catalytic rate constant k_c = 0.0031 (0.0001) s^{-1}, typically an order of magnitude smaller than the activation rate expected for the excitation conditions (extrapolating from Table 2). However, if we consider the autocatalytic reaction to occur in parallel with the initial elementary step of the CER, A → B, then the solution to the modified rate $dB/dt = k_aA + k_cAB$ provides a qualitatively better fit of $B(t)$ with an activation rate k_a = 0.015 (0.003) s^{-1} and little modification to the catalytic rate k_c = 0.0023 (0.0002) s^{-1}. In this instance, the activation rate is consistent with the wavelength dependence at 514 nm (Table 2) with half the power density. Evidently, this simplified scheme assumes no progression of the fluorescent fraction to the photobleached state, which is not unreasonable here since the sum of the initial dark and bright populations A_0 = 83 (2) and B_0 = 4.1 (0.5) obtained from the fit is close to that of the peak fluorescent QD population at the end of the illumination period, indicating that few (7−8) QDs have darkened or photobleached in this time. The observation of a fast and slow component to photoactivation is quite consistent with PLA studies on thin CdSe QD films,[39] where the slower rate of QY enhancement in the ensemble has been attributed to the passivation of the QD surface by the formation of a CdO layer under oxidative conditions. This process is normally associated with a reduction in PL efficiency due to the introduction of surface defects that act as nonradiative exciton recombination sites. However, it is possible that growth of the layer may shift exciton relaxation back to radiative decay in the core by forming a barrier to ionization and charge trapping in a similar way to the ZnS shell. The faster activation rate was attributed to the passivation of nonradiative decay centers at the surface by the physisorption of gas adsorbates, a process that is both rapid and reversible. A quasi-autocatalytic process has also been used to describe the formation of vacant surface sites on colloidal CdSe/ZnS *via* the desorption of the coordinating trioctylphosphine oxide ligand, TOPO, a process that was found to be mutually accelerated by photoionization.[45] Passivation of these vacant sites by more favorable adsorbates (solvent) or by slower oxide formation may then lead to rapid brightening and a slower PL enhancement, respectively. In this context, we associate the fast activation rate, k_a, with a reversible switching-on of QD fluorescence by the photoinduced, adsorbate-mediated passivation of surface defects. The catalytic rate, k_c, then reflects the slower and irreversible formation of an oxide layer that effectively compounds the function of the ZnS shell by raising a potential barrier to QD ionization and charge trapping.

Continued photooxidation ultimately leads to the decay in the fluorescent population observed with uninterrupted illumination and following multiple cycles of QD conditioning. In this case, defect formation will likely dominate any passivation effects by adsorbates or growth of the oxide layer, but degradation of the QD will also lead to a direct reduction in the excitation cross section with core size, a reduction in core size being evidenced by the observation of spectral bluing in the fluorescence of single QDs under continuous illumination.[16,43] It is also worth noting that the statistical aging associated with FI and the possibility that "off-times" extending beyond the experimental time window may contribute to a net decrease in the fluorescent QD population not accounted for here. It may contribute to small deviations in the experimentally measured fluorescent QD populations from the simple CER profile, but evidence indicates that PL decay from statistical aging follows an inverse power law[46] in time that is significantly slower than the photodarkening rates measured here. Furthermore, fluorescence recovery from the statistically darkened fraction would be expected following the cessation of continuous excitation, but this has not been observed in our controls. In the laser power regime used here, degradation of the fluorescent population closely follows the first-order exponential kinetics more commonly associated with irreversible photobleaching.

Autocatalytic PLA and QD Blinking. The physical picture emerging here is guided by the general consensus that the dark state, A, is associated with charging of the QD core, due to electron ionization and trapping with nonradiative, Auger-like quenching of subsequent excited electron−hole pairs.[9,47] In reality, electron ionization is in equilibrium with electron recombination, albeit one that is initially shifted toward oxidation of the core by light-driven ionizing processes. Continued excitation pushes this equilibrium back toward a

neutral, fluorescent core state, B. The mechanism by which this occurs is not well understood, but in addition to those explicitly involving charge displacement by adsorbates and surface passivation by oxide layer formation as described above, a number of other possibilities can be considered. Given that Auger recombination results in an excited charge carrier, its subsequent relaxation could lead to structural rearrangements of the QD that find their way to the surface, "annealing" defects and thus removing sites of nonradiative recombination, most likely irreversibly. Alternatively in a reversible sense, the Auger excited carrier can sample the QD surface more frequently, modulating the PL intensity *via* changes in the net core charge and raising the probability of surface trapping to render the core neutral and fluorescent. In addition, the reversible adsorption of polarizable molecules or counterions from the surrounding medium are likely to bias the QD surface potential in favor of a Coulomb blockade to electron ionization.[25] Although the equilibrium between dark A and bright B states is strongly driven toward activation, A → B under continuous illumination, the dynamic nature of the reversible processes described above allows both states A + B to coexist, at least within the time resolution of our experiment. The effect of this in FI is to reduce the effective brightness of the QD, potentially below detection limits, for a fixed signal integration time.[10] An alternative view is that partial modification of the surface leads to an immature QD with both A and B characteristics. Repeated transitions between the bright, fluorescent "on-state" and dark "off-state" catalyze the slow and irreversible modification of the QD to a fully mature, increasingly "on" state. The process is represented in the reaction scheme presented in Figure 5, which shows the competition between light-induced electron trapping (left-hand side) that rapidly photodarkens the QD and photoinduced processes that brighten the QD (right-hand side). In summary, the observation of a pseudo-autocatalytic photoactivation suggests that the on−off blinking associated with FI leads to a progressively more fluorescently active state, with more frequent and longer on-times that contribute to a time-averaged PLE from a dark, "undetectable" state to a fully, photoactivated state. The change in on/off time distributions would suggest a degree of correlation between consecutive on-times and off-time durations akin to the memory effects recently observed in QD blinking,[48,49] while a changing emission intensity is consistent with the measurement of a continuous distribution of emission states in QDs[50] and QY enhancement observed in single QD trajectories[16]

CONCLUSION

The kinetics of PL activation and decay in water-soluble ZnS-capped CdSe QDs have been investigated.

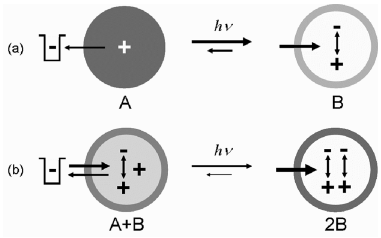

Figure 5. Schematic of (a) the parallel first-order and (b) pseudo-autocatalytic reactions describing photoactivation and enhancement at low excitation powers of <1 kW cm^{-2}. (a) Dark QD state, A (dark gray core), associated with ionization and core charging is transformed to the fluorescent state, B (white core), under continuous illumination by a photoinduced modification (light gray shell) that leads to a suppression in QD ionization. (b) Blinking accelerates surface modification (gray shell) and presents A + B (light gray core) together within the time resolution of the experiment. Repeated ionization and neutralization events catalyze the conversion of the immature dark state, A, to a fully active fluorescent state, B, with a strongly passivated surface (dark gray shell). Horizontal arrows associated with QDs indicate relative propensity for the electron to be ionized to a trap or be constrained in the QD core. Vertical arrows indicate radiative relaxation of exciton charge pairs, the number of which represents the relative intensity of monoexciton emission.

By imaging single QD fluorescence using TIRF microscopy, the evolution of the bright population within a dispersed ensemble has been measured directly under continuous illumination. By counting individual QDs, regardless of fluorescence intensity, PLA and population enhancement can be separated from PLE due to changes in the QY of individual QDs, which can be followed separately in the fluorescence trajectories of single QDs. Photoactivation of the dark fraction and decay of the bright fraction show kinetics that can be reasonably described by a simple CER reaction scheme, from which initial dark, A_0, and bright, B_0, populations, and rate constants for activation k_a and decay k_d can be readily obtained. Both rates show strong linear dependencies on excitation intensity between 1 and 10 kW cm^{-2}, while dark and bright fractions show anticorrelated behavior whereby their total remains near-constant over the same intensity range. The CER kinetics provide a useful measure of peak-detectable QD numbers, as well as totals and undetectable fractions, which may by applied to quantitative imaging. Analysis of PL reversibility shows that reactivation of the bright population arises largely from photoactivation of the dark fraction that remains at the end of an illumination cycle, albeit at a measurably faster rate that suggests QDs undergo a photoinduced "conditioning", even in their dark (undetectable) state. Loss of a photoactivatable dark fraction and photodarkening of the bright fraction results in few reactivated QDs common to multiple cycles of illumination at excitation intensities around 500 W cm^{-2}. At this power density, initial photoactivation is preceded by an induction period characteristic of an autocatalytic-like reaction. In this

case, the kinetics are described by the catalytic conversion of the dark state to the bright state through FI, whereby the photoinduced conditioning of the QD, by passivation of surface defects or other mechanisms, is accelerated by the electron ionization and neutralization processes associated with QD blinking. Importantly, the results provide compelling evidence for a fundamental link between FI and PLE that leads to PLA, all these being key optical properties that will ultimately affect the performance of QDs in a multitude of applications and devices.

METHODS

Sample Preparation. All experiments were conducted on borosilicate glass coverslips (22 mm, No. 0) cleaned in a UV-ozone chamber (PSD-II, Novascan) for 20 min to remove fluorescent residue. The slide was transferred to the microscope stage and optically coupled to the objective lens through index-matching immersion oil (n = 1.51, Nikon, UK). Samples were prepared from 2 μM stock solutions of streptavidin-functionalized ZnS/CdSe nanocrystals (80-0003, Invitrogen, UK) with a peak emission at 585 nm.

Dilutions in 0.1 M PBS (P-4417, Sigma-Aldrich) were optimized between 10^3 and 5×10^4-fold to yield surface densities of approximately 0.5 QDs/μm^2 at peak activation, as observed under TIRF. Then, 50 μL aliquots of diluted QDs were transferred to the sample coverslip and covered to prevent evaporation during analysis. At final QD concentrations of 1−2 nM, samples were found to be monodispersed and stable within the experimental time window (typically 5 min per acquisition), without significant loss or gain in population through desorption and adsorption of material at the surface. This was confirmed by QD fluorescence recovery after photobleaching (FRAP) experiments (see Supporting Information).

Instrumentation. Fluorescence imaging was performed using a modified inverted optical microscope (Nikon TE2000) coupled to an intensified charge-coupled device (ICCD) camera (IC-300, Photon Technology International). The microscope was configured to operate in a objective-type total internal reflection fluorescence (TIRF) mode with the spatially filtered, circularly polarized beam of a krypton−argon ion laser (Spectra Physics, BeamLok 165) as the excitation source. The laser was directed off a dichroic mirror (FF562-Di01, Semrock) through a high numerical aperture, oil-immersion objective lens (Plan Apochromat 100×, NA 1.4, Nikon) to the sample coverslip. Total internal reflection was achieved by focusing the laser at the back focal plane of the objective, off axis, such that the emergent beam at the sample interface was near-collimated and incident at an angle greater than the critical angle $\theta_c \sim 67°$ for a glass/water interface. This generated a 30 μm diameter TIRF footprint with power densities in the typically in the range of 1.2−12.5 kW cm^{-2} at the coverslip, accounting for near-field enhancement. Fluorescence was collected by the same objective and spectrally filtered from the excitation source, first by the long-pass dichroic mirror and second by a high transmission band-pass filter (FF562-Em, Semrock). The fluorescence image was finally projected onto the ICCD and captured using a PC-based frame grabber (AG-5, Scion Image Corp.).

Image Acquisition and Processing. Images were recorded as a 175 × 175 pixel stack of 3000 frames at 10 frames per second (fps) using Scion Image (Scion Image Corp.) and processed using ImageJ (http://rsb.info.nih.gov/ij/). Individual QD trajectories were averaged over a 3 × 3 grid of stacks spatially separated by 100 μm using a programmable scanning stage (Proscan II, Prior Scientific). Autofocusing, using a low-powered reference beam, was performed prior to the acquisition of each stack. The intensifier and video gain settings on the camera were optimized for minimum noise, maximum dynamic range, and fixed for all excitation intensities and wavelengths to allow direct comparisons.

Single QD Counting. A bespoke counting macro was designed to process the 8-bit grayscale image stacks in ImageJ. The algorithm initially establishes a background threshold for each image in a stack based upon the modal count and standard deviation of an end frame (photobleached) in a stack and the shot noise ($I^{1/2}$) in each frame. Counts above threshold are then considered fluorescence signal. For each frame in the stack, the intensity threshold is lowered sequentially from the maximum grayscale value in the image to the background threshold. Fluorescence peaks are positively identified and counted when a negative gradient exists between the peak pixel and >90% of pixels in the surrounding 5 × 5 array. The algorithm provides rapid identification of QDs, even where fluorescent peaks are not wholly resolved. A typical raw movie showing QD fluorescence activation and the corresponding movie of processed and binarized peaks are presented as Supporting Information.

QD Colocalization. To investigate the reversibility of PLE on QD populations and individual QD fluorescence trajectories, fluorescent peaks were colocalized between the image stacks accumulated for each cycle of illumination. In a first step following QD counting and image binarization, all QDs in each frame of each movie were projected onto a single image representing all detectable QDs in a single cycle. To account for the possibility of stage drift in xy between cycles, accumulated QD projections from consecutive cycles were systematically displaced relative to each other, pixel-by-pixel (±3 in x and y) to optimize particle overlap, as measured by the logical AND operation between images. The AND image is then used to colocalize QDs of a third cycle. Thus, QD populations common to cycles 1 AND 2, 2 AND 3, 1 AND 3, and 1 AND 2 AND 3 can be readily identified.

Acknowledgment. We thank the Royal Society for the award of a University Research Fellowship to M.O. during which this work was carried out and the School of Life Sciences for a awarding an EPSRC doctoral training assistant to S.L.

Supporting Information Available: Movie of single QD undergoing PLE, showing raw and processed; derivations of the consecutive elementary reactions scheme (CER) and parallel first-order and autocatalytic scheme fitting functions; control experiments. This material is available free of charge *via* the Internet at http://pubs.acs.org.

REFERENCES AND NOTES

1. Gao, X.; Cui, Y.; Levenson, R. M.; Chung, L. W. K.; Nie, S. *In Vivo* Cancer Targeting and Imaging with Semiconductor Quantum Dots. *Nat. Biotechnol.* **2004**, *22*, 969–976.
2. Michalet, X.; Pinaud, F. F.; Bentolila, L. A.; Tsay, J. M.; Doose, S.; Li, J. J.; Sundaresan, G.; Wu, A. M.; Gambhir, S. S.; Weiss, S. Quantum Dots for Live Cells, *In Vivo* Imaging, and Diagnostics. *Science* **2005**, *307*, 538–544.
3. Algar, W. R.; Tavares, A. J.; Krull, U. J. Beyond Labels: A Review of the Application of Quantum Dots as Integrated Components of Assays, Bioprobes, and Biosensors Utilizing Optical Transduction. *Anal. Chim. Acta* **2010**, *673*, 1–25.
4. Chon, J. W. M.; Zijlstra, P.; Gu, M.; van Embden, J.; Mulvaney, P. Two-Photon-Induced Photoenhancement of Densely Packed CdSe/ZnSe/ZnS Nanocrystal Solids and Its Application to Multilayer Optical Data Storage. *Appl. Phys. Lett.* **2004**, *85*, 5514–5516.
5. Uematsu, T.; Kimura, J.; Yamaguchi, Y. The Reversible Photoluminescence Enhancement of a CdSe/ZnS Nanocrystal Thin Film. *Nanotechnology* **2004**, *15*, 822–827.
6. Kamat, P. V. Quantum Dot Solar Cells. Semiconductor Nanocrystals as Light Harvesters. *J. Phys. Chem. C* **2008**, *112*, 18737–18753.
7. Kim, T.-H.; Cho, K.-S.; Lee, E. K.; Lee, S. J.; Chae, J.; Kim, J. W.; Kim, D. H.; Kwon, J.-Y.; Amaratunga, G.; Lee, S. Y.; Choi, B. L.; Kuk, Y.; Kim, J. M.; Kim, K. Full-Colour Quantum Dot

Displays Fabricated by Transfer Printing. *Nat. Photonics* **2011**, *5*, 176–182.
8. Nirmal, M.; Dabbousi, B. O.; Bawendi, M. G.; Macklin, J. J.; Trautman, J. K.; Harris, T. D.; Brus, L. E. Fluorescence Intermittency in Single Cadmium Selenide Nanocrystals. *Nature* **1996**, *383*, 802–804.
9. Efros, A. L.; Rosen, M. Random Telegraph Signal in the Photoluminescence Intensity of a Single Quantum Dot. *Phys. Rev. Lett.* **1997**, *78*, 1110–1113.
10. Hess, S. T.; Rochira, J. A.; Gudheti, M. V.; Gould, T. J.; Laughlin, R. R.; Nadeau, J. L. Fluorescence Intermittency Limits Brightness in CdSe/ZnS Nanoparticles Quantified by Fluorescence Correlation Spectroscopy. *J. Phys. Chem. C* **2007**, *111*, 1695–1708.
11. Nie, S. M.; Chan, W. C. W. Quantum Dot Bioconjugates for Ultrasensitive Nonisotopic Detection. *Science* **1998**, *281*, 2016–2018.
12. Clapp, A. R.; Medintz, I. L.; Mattoussi, H. Forster Resonance Energy Transfer Investigations Using Quantum-Dot Fluorophores. *ChemPhysChem* **2006**, *7*, 47–57.
13. Durisic, N.; Bachir, A. I.; Kolin, D. L.; Bates, I. R.; Grutter, P.; Wiseman, P. W. Effect of Quantum Dot Blinking on Diffusion Measurements Using Image Correlation Spectroscopy in Biological Systems. *Biophys. J.* **2007**, 518a–518a.
14. Cordero, S. R.; Carson, P. J.; Estabrook, R. A.; Strouse, G. F.; Buratto, S. K. Photo-activated Luminescence of CdSe Quantum Dot Monolayers. *J. Phys. Chem. B* **2000**, *104*, 12137–12142.
15. Jones, M.; Nedeljkovic, J.; Ellingson, R. J.; Nozik, A. J.; Rumbles, G. Photoenhancement of Luminescence in Colloidal CdSe Quantum Dot Solutions. *J. Phys. Chem. B* **2003**, *107*, 11346–11352.
16. Lee, S. F.; Osborne, M. A. Photodynamics of a Single Quantum Dot: Fluorescence Activation, Enhancement, Intermittency, and Decay. *J. Am. Chem. Soc.* **2007**, *129*, 8936–8937.
17. Sun, Y. H.; Liu, Y. S.; Vernier, P. T.; Liang, C. H.; Chong, S. Y.; Marcu, L.; Gundersen, M. A. Photostability and pH Sensitivity of CdSe/ZnSe/ZnS Quantum Dots in Living Cells. *Nanotechnology* **2006**, *17*, 4469–4476.
18. Zhang, C.-Y.; Yang, K. Accurate Detection of On-State Quantum Dot and Biomolecules in a Microfluidic Flow with Single-Molecule Two-Color Coincidence Detection. *Anal. Bioanal. Chem.* **2010**, *397*, 703–708.
19. Ebenstein, Y.; Mokari, T.; Banin, U. Fluorescence Quantum Yield of CdSe/ZnS Nanocrystals Investigated by Correlated Atomic-Force and Single-Particle Fluorescence Microscopy. *Appl. Phys. Lett.* **2002**, *80*, 4033–4035.
20. Yao, J.; Larson, D. R.; Vishwasrao, H. D.; Zipfel, W. R.; Webb, W. W. Blinking and Nonradiant Dark Fraction of Water-Soluble Quantum Dots in Aqueous Solution. *Proc. Natl. Acad. Sci. U.S.A.* **2005**, *102*, 14284–14289.
21. Krauss, T. D.; Brus, L. E. Charge, Polarizability, and Photoionization of Single Semiconductor Nanocrystals. *Phys. Rev. Lett.* **2000**, *84*, 1638–1638.
22. Oda, M.; Hasegawa, A.; Iwami, N.; Nishiura, K.; Ando, N.; Nishiyama, A.; Horiuchi, H.; Tani, T. Photoluminescence Behaviors of Single CdSe/ZnS/TOPO Nanocrystals: Adsorption Effects of Water Molecules onto Nanocrystal Surfaces. *J. Lumin.* **2007**, *127*, 198–203.
23. Tice, D. B.; Frederick, M. T.; Chang, R. P. H.; Weiss, E. A. Electron Migration Limits the Rate of Photobrightening in Thin Films of CdSe Quantum Dots in a Dry N_2 (g) Atmosphere. *J. Phys. Chem. C* **2011**, *115*, 3654–3662.
24. Asami, H.; Abe, Y.; Ohtsu, T.; Kamiya, I.; Hara, M. Surface State Analysis of Photobrightening in CdSe Nanocrystal Thin Films. *J. Phys. Chem. B* **2003**, *107*, 12566–12568.
25. Maenosono, S. Modeling Photoinduced Fluorescence Enhancement in Semiconductor Nanocrystal Arrays. *Chem. Phys. Lett.* **2003**, *376*, 666–670.
26. Park, S. J.; Link, S.; Miller, W. L.; Gesquiere, A.; Barbara, P. F. Effect of Electric Field on the Photoluminescence Intensity of Single CdSe Nanocrystals. *Chem. Phys.* **2007**, *341*, 169–174.
27. Lee, J. D.; Maenosono, S. Field-Induced Control of Universal Fluorescence Intermittency of a Quantum Dot Light Emitter. *J. Chem. Phys.* **2010**, *133*, 074703–074709.
28. Osborne, M. A.; Lee, S. F. Brightening, Blinking, Bluing and Bleaching in the Life of a Quantum Dot: Friend or Foe? *ChemPhysChem* **2009** *10*, 2174–2191.
29. Bu, X.; Chen, H.; Gai, H.; Yang, R.; Yeung, E. S. Scattering Imaging of Single Quantum Dots with Dark-Field Microscopy. *Anal. Chem.* **2009**, *81*, 7507–7509.
30. Zhelev, Z.; Jose, R.; Nagase, T.; Ohba, H.; Bakalova, R.; Ishikawa, M.; Baba, Y. Enhancement of the Photoluminescence of CdSe Quantum Dots During Long-Term UV-Irradiation: Privilege or Fault in Life Science Research? *J. Photochem. Photobiol. B* **2004**, *75*, 99–105.
31. Jin, W. J.; Fernandez-Arguelles, M. T.; Costa-Fernandez, J. M.; Pereiro, R.; Sanz-Medel, A. Photoactivated Luminescent CdSe Quantum Dots as Sensitive Cyanide Probes in Aqueous Solutions. *Chem. Commun.* **2005**, 883–885.
32. Clarke, S. J.; Hollmann, C. A.; Zhang, Z. J.; Suffern, D.; Bradforth, S. E.; Dimitrijevic, N. M.; Minarik, W. G.; Nadeau, J. L. Photophysics of Dopamine-Modified Quantum Dots and Effects on Biological Systems. *Nat. Mater.* **2006**, *5*, 409–417.
33. Gur, I.; Fromer, N. A.; Geier, M. L.; Alivisatos, A. P. Air-Stable All-Inorganic Nanocrystal Solar Cells Processed from Solution. *Science* **2005**, *310*, 462–465.
34. Lounis, B.; Bechtel, H. A.; Gerion, D.; Alivisatos, P.; Moerner, W. E. Photon Antibunching in Single CdSe/ZnS Quantum Dot Fluorescence. *Chem. Phys. Lett.* **2000**, *329*, 399–404.
35. Htoon, H.; Malko, A. V.; Bussian, D.; Vela, J.; Chen, Y.; Hollingsworth, J. A.; Klimov, V. I. Highly Emissive Multiexcitons in Steady-State Photoluminescence of Individual "Giant" CdSe/CdS Core/Shell Nanocrystals. *Nano Lett.* **2010**, *10*, 2401–2407.
36. Spinicelli, P.; Buil, S.; Quelin, X.; Mahler, B.; Dubertret, B.; Hermier, J. P. Bright and Grey States in CdSe–CdS Nanocrystals Exhibiting Strongly Reduced Blinking. *Phys. Rev. Lett.* **2009**, *102*, 136801–136804.
37. Nesbitt, D. J.; Peterson, J. J. Modified Power Law Behavior in Quantum Dot Blinking: A Novel Role for Biexcitons and Auger Ionization. *Nano Lett.* **2009**, *9*, 338–345.
38. Cordones, A. A.; Bixby, T. J.; Leone, S. R. Evidence for Multiple Trapping Mechanisms in Single CdSe/ZnS Quantum Dots from Fluorescence Intermittency Measurements over a Wide Range of Excitation Intensities. *J. Phys. Chem. C* **2011**, *115*, 6341–6349.
39. Javier, A.; Strouse, G. F. Activated and Intermittent Photoluminescence in Thin CdSe Quantum Dot Films. *Chem. Phys. Lett.* **2004**, *391*, 60–63.
40. Wang, Y.; Tang, Z. Y.; Correa-Duarte, M. A.; Pastoriza-Santos, I.; Giersig, M.; Kotov, N. A.; Liz-Marzan, L. M. Mechanism of Strong Luminescence Photoactivation of Citrate-Stabilized Water-Soluble Nanoparticles with CdSe Cores. *J. Phys. Chem. B* **2004**, *108*, 15461–15469.
41. Colvin, V. L.; Alivisatos, A. P. Cdse Nanocrystals with a Dipole-Moment in the 1st Excited-State. *J. Chem. Phys.* **1992**, *97*, 730–733.
42. Nazzal, A. Y.; Wang, X. Y.; Qu, L. H.; Yu, W.; Wang, Y. J.; Peng, X. G.; Xiao, M. Environmental Effects on Photoluminescence of Highly Luminescent CdSe and CdSe/ZnS Core/Shell Nanocrystals in Polymer Thin Films. *J. Phys. Chem. B* **2004**, *108*, 5507–5515.
43. van Sark, W. G. J. H. M.; Frederix, P. L. T. M.; Bol, A. A.; Gerritsen, H. C.; Meijerink, A. Blueing, Bleaching, and Blinking of Single CdSe/ZnS Quantum Dots. *ChemPhysChem* **2002**, *3*, 871–879.
44. Katari, J. E. B.; Colvin, V. L.; Alivisatos, A. P. X-ray Photoelectron-Spectroscopy of Cdse Nanocrystals with Applications to Studies of the Nanocrystal Surface. *J. Phys. Chem.* **1994**, *98*, 4109–4117.
45. Komoto, A.; Maenosono, S. Photoinduced Fluorescence Intensity Oscillation in a Reaction-Diffusion Cell Containing a Colloidal Quantum Dot Dispersion. *J. Chem. Phys.* **2006**, *125*, 114705–114716.
46. Brokmann, X.; Hermier, J. P.; Messin, G.; Desbiolles, P.; Bouchaud, J. P.; Dahan, M. Statistical Aging and Nonergodicity in the Fluorescence of Single Nanocrystals. *Phys. Rev. Lett.* **2003**, *90*, 120601–120605.

47. Frantsuzov, P.; Kuno, M.; Janko, B.; Marcus, R. A. Universal Emission Intermittency in Quantum Dots, Nanorods and Nanowires. *Nat. Phys.* **2008**, *4*, 519–522.
48. Stefani, F. D.; Zhong, X. H.; Knoll, W.; Han, M. Y.; Kreiter, M. Memory in Quantum-Dot Photoluminescence Blinking. *New J. Phys.* **2005**, *7*, 197–214.
49. Janko, B.; Volkan-Kacso, S.; Frantsuzov, P. A. Correlations between Subsequent Blinking Events in Single Quantum Dots. *Nano Lett.* **2010**, *10*, 2761–2765.
50. Zhang, K.; Chang, H. Y.; Fu, A. H.; Alivisatos, A. P.; Yang, H. Continuous Distribution of Emission States from Single CdSe/ZnS Quantum Dots. *Nano Lett.* **2006**, *6*, 843–847.